Journal of Materials Chemistry A

RSC Publishing

FEATURE ARTICLE

View Article Online
View Journal | View Issue

Cite this: *J. Mater. Chem. A*, 2013, **1**, 11513

Coaxial electrospun nanostructures and their applications

Honglin Qu,[a] Suying Wei*[b] and Zhanhu Guo*[a]

Received 19th June 2013
Accepted 4th July 2013

DOI: 10.1039/c3ta12390a

www.rsc.org/MaterialsA

As an innovative extension of electrospinning, coaxial electrospinning could be used to fabricate polymer nanofibers with unique core–sheath or hollow structures. In this review, the effects of both internal and external factors on the fibers are briefly introduced. In addition to the inherent parent polymer properties, various nanoparticles, metal salts and other materials could be added to the polymer matrix to achieve integrated multi-functions. The preparation of carbon, ceramic and metal nanofibers from co-axial electrospinning is reviewed. With a large specific surface area, high mechanical strength and other unique properties, their applications in energy storage, luminescence, catalysis and filtration are critically reviewed with detailed examples.

1 Introduction

With optimized electrospinning parameters including polymer concentration, solution conductivity, applied voltage, flow rate and collection distance, the fiber size can be decreased to several nanometers. For example, Phone *et al.*[1] have fabricated polyvinyl alcohol fibers with dimensions varying from 40 to 80 nm. Huang *et al.*[2] and Zhou *et al.*[3] have even reported fibers with sizes of 1.6 and 5 nm. Electrospinning can be applied to process polymers, ceramics, metals, semiconductors and their composites (matrix and nanofillers) to fibers. To broaden the nanofiber properties, researchers have introduced extra phases to construct core–sheath or hollow structures with desired multi-functions. And compared with single structure fibers, the core–sheath fibers possess more attractive merits including controllable mechanical strength, and better thermal and electrical conductivities.[4–8] Different methods have been reported to prepare core–sheath structures, such as the fiber template method, the emulsion electrospinning method, direct electrospinning and coaxial electrospinning methods.[9,10] The fiber template method uses the prepared fibers as a template and coats sheath materials on their surface by chemical vapor deposition, plasma or sol–gel coating methods.[11–17] However, this method needs two steps and it is difficult to control the fiber dimension with this method. The last three methods are based on the electrospinning process. The emulsion

[a]*Integrated Composites Laboratory (ICL), Dan F Smith Department of Chemical Engineering, Lamar University, Beaumont, TX 77710, USA. E-mail: zhanhu.guo@lamar.edu; Tel: +1 409 880 7654*

[b]*Department of Chemistry and Biochemistry, Lamar University, Beaumont, TX 77710, USA. E-mail: suying.wei@lamar.edu; Tel: +1 409 880 7976*

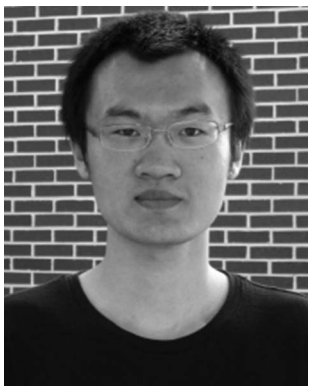

Mr Honglin Qu is currently a Ph.D. student in the Dan F. Smith Department of Chemical Engineering at Lamar University studying under Prof. Zhanhu Guo. He received a BE degree in Chemical Engineering from the East China University of Science and Technology (2012). His research interests focus on the electrospinning process, synthesis of carbon based nanocomposites, especially graphene oxide and carbon nanofibers, and their applications in energy storage, electronic devices and environmental remediation.

Dr Suying Wei, currently an Assistant Professor in the Department of Chemistry and Biochemistry at Lamar University, obtained a Ph.D. degree in chemistry from the Louisiana State University (2006), a MS degree in applied chemistry from the Beijing University of Chemical Technology (2000) and a BS degree in chemical engineering from the Shandong University of Science and Technology (1996). Her research interests are in multifunctional composites especially those for biomedical applications. Her expertise is in analytical, materials and surface chemistry.

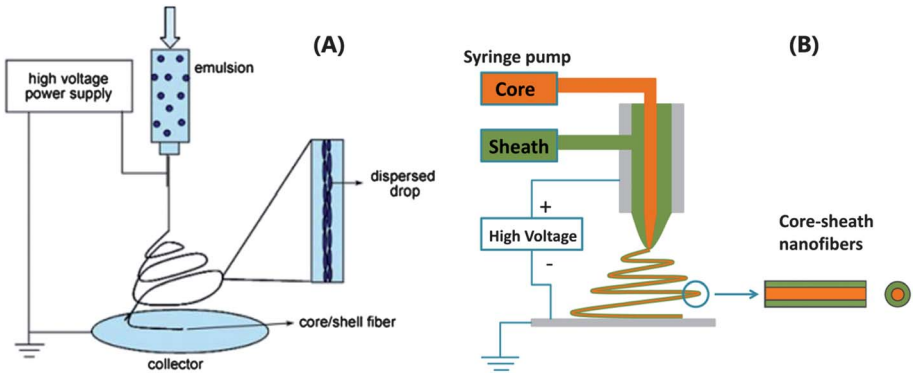

Fig. 1 The schematic diagram of (A) emulsion electrospinning setup for core–sheath fibers. Reprinted with permission from Springer.[10] (B) Co-axial electrospinning setup for core–sheath fibers.

electrospinning method depends on the immiscibility of the prepared solution, which can cause the separation of different materials. The minor materials exist as droplets in the suspension. Individual droplets can agglomerate to form the core phase when they are pumped out,[18] Fig. 1(A). Though very simple,[12,19,20] it is not stable or universal. The direct electrospinning method is generally only used for preparing hollow fibers.[4,5,21–23] It utilizes the oxygen concentration gradient during the annealing process to impel the diffusion of the metal precursor to the surface and the hollow fibers are formed after decomposition. However, this method cannot control the diameter and usually leaves some defects on the fiber surface.

Compared with the above two methods, coaxial electrospinning, first demonstrated by Loscertales *et al.* in 2002,[24] could provide production stability due to its specially designed multi-channel spinneret consisting of core and sheath channels for the core–sheath structure to be constructed spontaneously. Under a sufficient electrical field, the core–sheath jets get ejected and after a perturbed electrospinning process, the core–sheath nanofibers will be collected. The coaxial electrospinning setup is schematically shown in Fig. 1(B). Coaxial electrospinning depends on the same parameters as those in the conventional one. However, additional phases introduce an interface interaction (miscibility and stress due to the viscosity difference) and the individual physical behavior of different phases (solidification and conductivity) also complicates the coaxial electrospinning. During the spinning, the sheath layer could act as a barrier to retard the evaporation of inside materials and ensure a smooth mass transfer.[25–27] And jets can keep the liquid phase longer to complete a proper elongation process. The sheath phase can also encapsulate some non-spinnable core materials[28,29] and lubricate the spinning head for concentrated polymer core solutions.[30,31] The concentrations of both phases should exceed a critical value to maintain a uniform morphology.[32] And it also affects the fiber dimension. The increase of both core and sheath flow rates can enlarge their corresponding phases and total dimensions.[33,34] Due to the core–sheath encapsulation structure, both flow rates should be matched. At very small core–sheath flow rate ratios, an insufficient core solution cannot support a continuous smooth core phase. By increasing its flow rate, the core phase will become consecutive and thicker. However, excessive core materials will form pendant droplets.[35] If the applied voltage is very low, gravity cannot be ignored as compared with the electrical force. The pumped solution will drop down and, because the applied voltage is low, electrostatic force is not sufficient to draw the whole liquid out. As a result, only the outer part, sheath, can be handled into jets. As the voltage increases, successful drawing and efficient elongation process can be achieved.[36] But excessively high voltage could increase the environmental temperature and lead to poor electrospinnability.[37,38] Addition of a salt could intensify the conductivity and result in more charges. The intensified and uniform whipping effect could decrease the fiber defects.[16,39] However, a too high salt loading will affect polymer dissolution as well as solution uniformity. The longer the collection distance is, the longer whipping process the jets can experience, and thus the fibers can get sufficiently elongated.[30] But the excessively long collection distance can lead to the disappearance of the surface charge and the weakened electrical field is adverse for the electrospinning process.

With the removal of the core phase, the specific surface area has been enlarged significantly to nearly 200%, which enhanced their performance in sensors, filtration, and lithium ion

Dr Zhanhu Guo, currently an Assistant Professor of Chemical Engineering and Director of Integrated Composites Laboratory (ICL) at Lamar University, obtained a Ph.D. degree in Chemical Engineering from the Louisiana State University (2005) and received three-year post-doctoral training at the Mechanical and Aerospace Engineering Department in the University of California Los Angeles. His current research covers fundamentals of multifunctional nanocomposites for electronic devices and environmental remediation applications.

batteries.[40–42] To obtain hollow nanofibers, an extraction process[43] or a thermal treatment[44] is needed. In an extraction process, mineral oil or aqueous polymer solutions are normally used as core materials.[32,45] However, it takes a long time to complete the extraction process, usually overnight or even a whole day. And some residuals and impurities will always be left. Thermal treatment is a quicker and more direct method, and can be combined with additional heat treatments to make it more efficient. Chen *et al.*[44] reported amorphous carbon nanotubes. During thermal treatment, mineral oil gets burned out and the sheath polyacrylonitrile (PAN)/polyvinylpyrrolidone (PVP) composites convert to carbon and the metal precursor, nickel acetate $Ni(Ac)_2$, decomposes to metal particles.

Generally, the core–sheath fibers are a little larger than those obtained from conventional electrospinning.[46,47] Some researchers[48,49] have obtained core–sheath fibers from coaxial spinning with a diameter of around 200 nm. Sun *et al.*[29] have reported fibers with a diameter of 66 nm by tuning the composition and operating conditions. Different materials can be integrated into core or sheath phases with desired functions and nanofibers with two unique nanostructures have been developed possessing amazing properties.

In the last five years, more than two hundred papers on coaxial electrospinning and their applications, especially in energy and tissue engineering fields, have been published.[50–53] But to the best of our knowledge, only two review papers on the coaxial electrospinning technique have been published, in which no energy and other applications were reported.[37,54] A systematic review of this advanced technique together with its unique applications will help scientists to get familiar with its broad spectrum of applications. In this review, the coaxial electrospinning technique and its characteristics, especially the interaction between the two phases, are briefly delineated. The applications of the coaxial electrospun core–sheath as well as hollow fibers in catalysis, energy, filtration and other fields are critically reviewed with detailed examples.

2 Applications

Due to their excellent physicochemical properties and flexible characteristics, coaxial electrospun core–sheath or hollow fibers can be used in various fields. For example, core–sheath fibers can exhibit an enhanced mechanical property compared to simple fibers, such as silk fibroin-silk sericin core–sheath fibers[36] with a breaking strength of 1.93 MPa and a breaking energy of 7.21 J kg^{-1}, which are 82% and 92.8% higher than those of single silk fibroin fibers. To illustrate more specifically, in this section, the applications of these fibers in the fields including lithium ion batteries, solar cells, luminescence, supercapacitors, photocatalytic environmental remediation and filtration are critically reviewed with examples and design principles.

2.1 Lithium ion batteries

Right now, the whole society faces a serious energy challenge with traditional fossil energy being used up and other new energies not ready for large scale deployment. The widely used internal combustion engine utilizing fossil energy has faced a bottleneck in the energy field development due to its low energy conversion resulting from its low energy efficiency, normally less than 30%. And the combustion of fossil fuels can cause severe environmental pollution. Urged by all these problems, scientists turn to a high-grade sustainable clean energy, electricity. And among the energy storage devices, batteries have been in the spotlight attracting considerable attention. Among all the batteries, the lithium ion battery has become the primary candidate in many applications, such as communication, transportation and regenerated energy sectors[55] due to its higher voltage (about 3.6 V, two times higher than that of aqueous batteries), gravimetric specific energy (about 240 W h kg^{-1}, six times higher than that of lead acid batteries), long duration (500–1000 cycles), wide temperature range (−20 to 60 °C) and minimum memory effect.[56,57] Fig. 2 shows the schematic diagram of a typical commercial lithium ion battery with lithium alloy compound and graphite as the cathode and the anode, respectively. After the circuit is connected, electrons will flow from the anode to the cathode through an external circuit forming current driven by the chemical potential difference between the electrode materials, at the same time, lithium ions are transported in the same direction through the electrolyte inside the battery. At the cathode, lithium ions react with cathode material and electrons, and deposit there. During the charging process, both electrons and lithium ions go back though the previous pathway driven by the applied potential difference.[58] Through the charge–discharge process, the stored chemical energy is finally converted into electricity. The chemical reactions during the charging and discharging processes are listed.[59]

$$\text{Cathode}: \frac{1}{2}\text{Li}^+ + \frac{1}{2}\text{e}^{-1} + \text{Li}_{0.5}\text{CoO}_2 \underset{\text{charge}}{\overset{\text{discharge}}{\rightleftharpoons}} \text{LiCoO}_2$$

$$\text{Anode}: \text{LiC}_6 \underset{\text{charge}}{\overset{\text{discharge}}{\rightleftharpoons}} \text{Li}^+ + \text{e}^- + \text{C}_6$$

During the charging process, the lithium ions will insert into the graphite layer and combine with carbon atoms. This requires that the anode material should provide an extremely

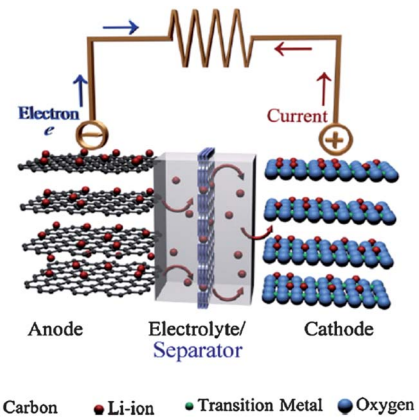

Fig. 2 Schematic illustration of a typical lithium-ion battery with graphite and $LiCoO_2$ as anode and cathode materials, respectively. Reprinted with permission from Elsevier.[58]

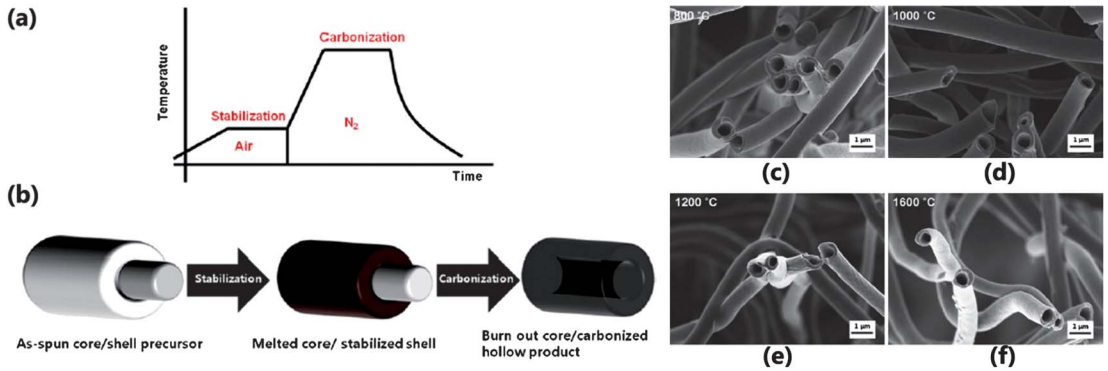

Fig. 3 (a) The schematic thermal treatment profile and (b) structure evolution of the as-spun fibers during thermal treatment and FE-SEM images of HCNFs carbonized at (c) 800, (d) 1000, (e) 1200 and (f) 1600 °C. Reprinted with permission from Elsevier.[63]

large surface area for a convenient combination. On the other hand, the insertion of lithium ions could cause electrode volume expansion, which affects the electric contact and battery capacity. And this expansion is a very serious problem in all lithium batteries. Therefore, different electrode materials have been studied aiming to eliminate the side-effect of the volume expansion and to support enough active sites. Hollow nanofibers are excellent candidates as anode material for lithium ion batteries. The hollow structure not only possesses very high specific surface area, but also buffers the volume expansion during the lithiation process. And the hollow structure can integrate various components together to promote the performance of the lithium ion battery.

Graphite carbon is a very common commercial anode material for lithium ion batteries,[55] but due to its low capacity and safety issues, other materials including transition metals, semiconductors and lithium alloys have been studied.[60,61] Generally, carbon material is an excellent choice for an electrode in the battery system and it can be classified into graphitic (soft) and non-graphitic (hard) carbon. Specifically, soft carbon possesses a well-ordered lamellar structure, while hard carbon displays a relatively turbostatic arrangement. And significant property differences as the lithium ion battery anode result due to the structural diversity.[62] Hard carbon possesses a high capacity (400–500 mA h g^{-1}), but poor capacity retention performance, which means that the high capacity will get attenuated very soon. Compared with hard carbon, soft carbon has a lower, but reversible capacity (200–300 mA h g^{-1}), however, it shows a very serious voltage hysteresis during the delithiation process, in which lithium ions are desorbed from the anode. A combination of the advantages of both materials can enhance the performance of lithium ion batteries and the coaxial electrospinning technique has been reported to achieve this goal.

Other scientists considered adding other components to enhance the performance. With a high theoretical capacity of about 4000 mA h g^{-1}, nearly ten times that of the commercial graphite anode, silicon has been integrated into electrodes to improve the lithium ion battery performance.[64–66] TiO_2 is another good choice due to its low cost, high working voltage, and structural stability during lithium insertion and extraction processes, although it has some drawbacks, it still attracts the attention.[67–69] SnO_2 is also an excellent anode material due to its higher capacity (about 800 mA h g^{-1}) than that of graphite, high charge and discharge capacity, and fast electron transportation.[70,71] All these materials could be fabricated into hollow composite nanofibers as anodes for lithium ion batteries to enhance their performance.

Lee *et al.*[63] have utilized coaxial electrospinning to fabricate hollow carbon nanofibers as anode materials and studied the carbonization temperature effect on the electrochemical

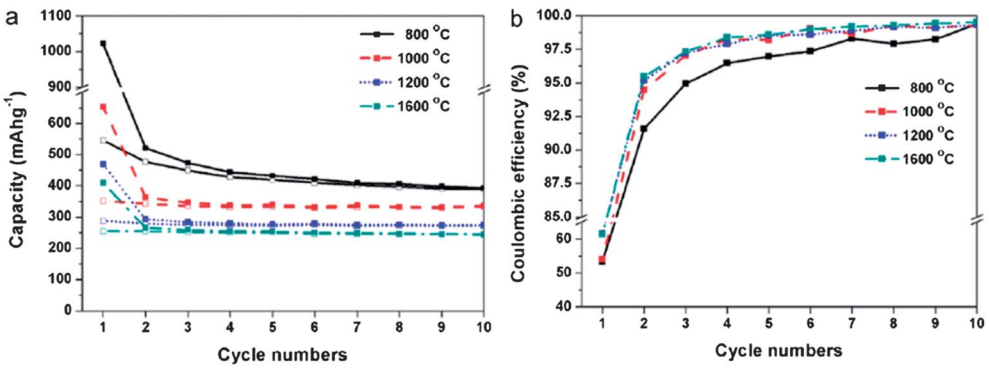

Fig. 4 Cycle performance of HCNGs carbonized at various temperatures under a current density of 50 mA g^{-1}, (a) charge–discharge capacity and (b) coulombic efficiency. Reprinted with permission from Elsevier.[63]

performance. Both styrene-*co*-acrylonitrile (SAN) and PAN are good choices as carbon precursors and their DMF solutions serve as the core and sheath solution, respectively. The as-spun fibers experienced a one-hour stabilization process at 270–300 °C in an air atmosphere and a following one-hour carbonization at 800, 1000, 1200, 1600 °C in a nitrogen atmosphere, Fig. 3(a). During stabilization, the linear PAN molecules were converted to the ladder structure and got carbonized in the following process, at the same time, the core phase burned out resulting in the tubular structure, Fig. 3(b). The morphologies of the fibers carbonized at different temperatures are shown in Fig. 3(c)–(f). And the capacities after 10 cycles were 390, 334, 273 and 243 mA h g^{-1}, corresponding to the carbonization temperatures of 800, 1000, 1200, 1600 °C, with a very high coulombic efficiency (the ratio of output charge to input charge), Fig. 4.

Liu *et al.*[72] reported a core–sheath soft–hard carbon nanofiber web, which displayed an improved electrochemical performance as an anode in the lithium ion battery. A special terpolymer fibril (93 wt% acrylonitrile, 5.3 wt% methylacrylate and 1.7 wt% itaconic acid) in DMF served as the sheath solution and mineral oil as the core solution. The as-spun fibers were stabilized for 6.5 h at 270 °C in an air atmosphere and then carbonized for 1 h at 850 °C under nitrogen protection. Finally, the soft–hard core–sheath carbon nanofibers were obtained with sheath PAN converted to hard carbon and core mineral oil decomposed to amorphous soft carbon. In this anode configuration, the hard sheath could prevent the deformation of soft core, which dominated the stable reverse capacity after a long service time. And an enhanced reversible capacity was obtained, 520, 450 and 390 mA h g^{-1} after 20 cycles at 25, 50 and 100 mA g^{-1}, respectively.

Lee *et al.*[42] have studied the electrochemical performance of the Si–C core–sheath fibers as the lithium ion battery anode. The fibers were prepared by following similar procedures[63] and are briefly stated as follows. The Si nanoparticles with a diameter smaller than 100 nm were added to the core solution. The as-spun nanofibers were stabilized at 270–300 °C for one-hour in an air atmosphere and carbonized at 1000 °C for one-hour in a nitrogen atmosphere with a heating speed of 10 °C min^{-1}. PAN converted to a carbon sheath and Si nanoparticles attached onto the inner wall of hollow fibers. Si–C hollow fibers are formed. Fig. 5 illustrates the volume expansion mechanisms during the lithiation process. Due to the large d-space between turbostratic carbon layers, the electrode volume expansion could be caused by the combination of Si and lithium ions. The anode material showed an improved reversible capacity of 244 mA h g^{-1} with a 92% capacity retention after 50 cycles and a 98% coulombic efficiency after 10 cycles, Fig. 6.

Hwang *et al.*[73] have fabricated core–sheath fibers containing different loadings of Si in the carbon core matrix as the anode for lithium ion batteries. Specifically, PAN was the sheath material, and poly(methyl methacrylate) (PMMA) and silicon nanoparticles were core materials. DMF served as a solvent for both phases. Proper quantity of acetone (acetone : DMF = 1 : 1, w : w) was also added to the core solution to prevent the mixing of core and sheath materials. PMMA worked as a stabilizer to encapsulate silicon nanoparticles and left enough space after burning out to buffer the volume expansion during the charging process. The as-spun fibers were stabilized at 280 °C for 1 h in an air atmosphere and further carbonized at 1000 °C for 5 h in argon. The electrode was prepared as follows: about 70 wt% electrospun fibers, 15 wt% super P and 15 wt% poly(acrylic acid) (PAA) were mixed and added to 1-methyl-2-pyrrolidinone (NMP) to form slurry, which was then pasted onto a copper current collector. The prepared electrode was dried in a vacuum oven at 70 °C for 6 h and then punched into circular discs. The effect of silicon integrated in the samples on the battery capacity was studied, Fig. 7(a). The more weight percent of silicon was added, the higher discharge capacity the samples had demonstrated. This is due to the superior capacity of silicon itself. As shown for the sample with 50 wt% Si through its voltage profile in Fig. 7(b) and (c), its capacity was very high, 1491 and 1305 mA h g^{-1}, in the first charging and discharging process at 0.137 A g^{-1}. And the performance of the electrode was very stable even after 300 cycles.

For comparison, two more control materials have been prepared with the same method as electrodes. The first one was bare silicon nanoparticles with super P and the second one was carbon fibers decorated with Si nanoparticles. Compared with these two control electrodes, the desired electrode exhibited a high discharge capacity around 1250 mA h g^{-1} with a nearly 100% retention in the first 100 cycles at 0.242 A g^{-1} current rate. With further increase in the current rate up to 2.748 and 6.89 A g^{-1}, the electrode could still display a rather stable capacity in a larger cycle period with 99% retention after 300 cycles and 80.9% retention after 1500 cycles, Fig. 7(d)–(f). This improved electrode performance is due to the extremely high theoretical specific capacity of silicon, nearly 4000 mA h g^{-1}, which is about

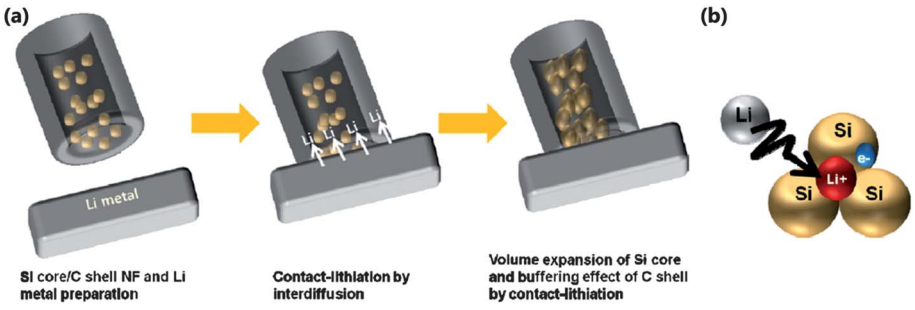

Fig. 5 The schematic diagram of (a) volume expansion behavior during contact-lithiation and (b) ionization of Li atoms in the Si matrix. Reprinted with permission from Elsevier.[42]

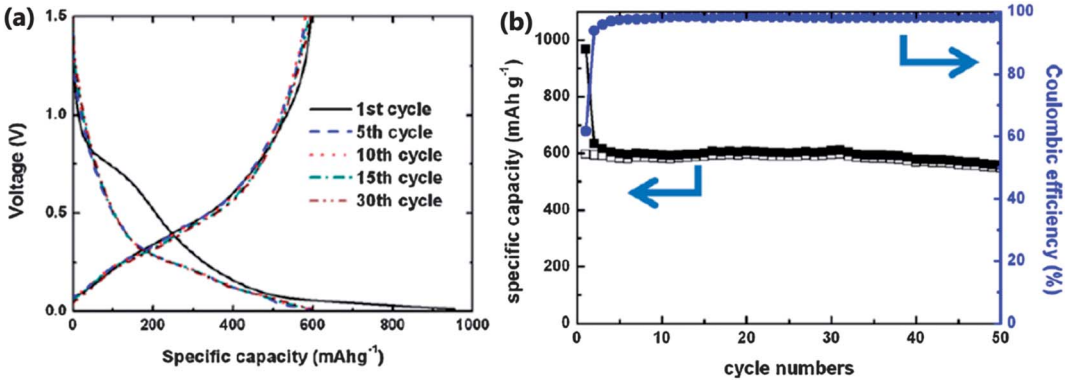

Fig. 6 Cycling performances of Si–C core–shell nanofibers, (a) voltage profiles at different cycles and (b) coulombic efficiency and specific capacity–cycle number curve. Reprinted with permission from Elsevier.[42]

ten times higher than those of commercial graphite anodes. And the performance is also determined by the stability of the solid electrolyte interphase (SEI) and the contact between Si nanoparticles and carbon matrix. Because the Si volume expansion at high current rate was not that considerable, the SEI layers were more stable and thus more reversible charge–discharge reaction occurred.

Han *et al.*[68] have investigated TiO_2 as the anode for lithium ion batteries. An improved electrochemical performance of the TiO_2 hollow fibers and nitridated TiO_2 hollow fibers was reported than that of solid ones. $Ti(OiPr)_4$ was used as a titanium precursor and PVP as a stabilizer in the sheath phase, and mineral oil was used as the core phase. After natural drying, extraction of mineral oil and calcination, hollow fibers were obtained. The nitridation step was processed through another annealing treatment under ammonia and the related schematic morphology changes are shown in Fig. 8a–c.

The solid, hollow and nitridated hollow TiO_2 nanofibers exhibited initial coulombic efficiencies of 75.8, 77.1 and 86.8%, and capacity retentions of 96.8, 98.8 and 100% after 100 cycles. And at different current rates, hollow fibers exhibited a higher capacity than solid fibers, Fig. 9. This improved performance is due to the larger surface area (around 25%) for lithium ions to combine with active materials, and the decreased diffusion length of the lithium ions down to nearly 50%. The diffusion length is the maximum distance, through which lithium ions must diffuse to combine with anodic materials. Therefore, the longer the diffusion distance is, the more adverse it is for the performance of the lithium ion battery. And the high conductivity of the nitridated hollow nanofibers will also benefit its performance. The enhanced anode stability arises from the hollow structure, which provides space for volume expansion during lithiation.

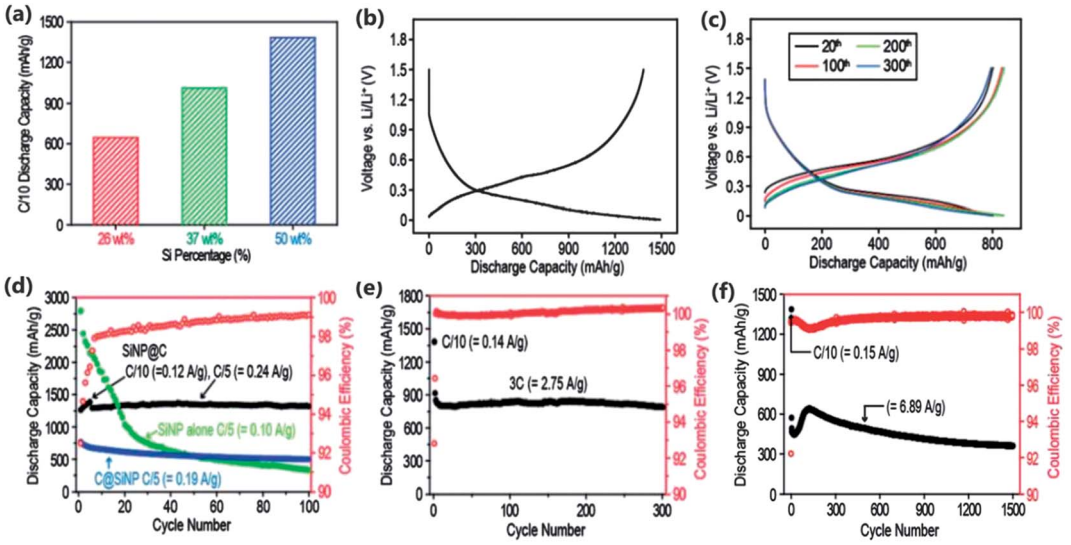

Fig. 7 (a) Discharge capacities of the fabricated electrodes with different Si loadings at 0.1 C rate; (b) potential profiles of the fabricated electrode with 50 wt% Si during the first cycle at 0.137 A g^{-1}; (c) potential profiles of the fabricated electrode with 50 wt% Si at different cycles at 2.749 A g^{-1}; (d) cycle performance of the fabricated electrode and control electrodes at 0.242 A g^{-1}; (e) cycle performance of the fabricated electrode at 2.748 A g^{-1}; (f) cycle performance of the fabricated electrode and control electrodes at 6.887 A g^{-1}. Reprinted with permission from American Chemical Society.[73]

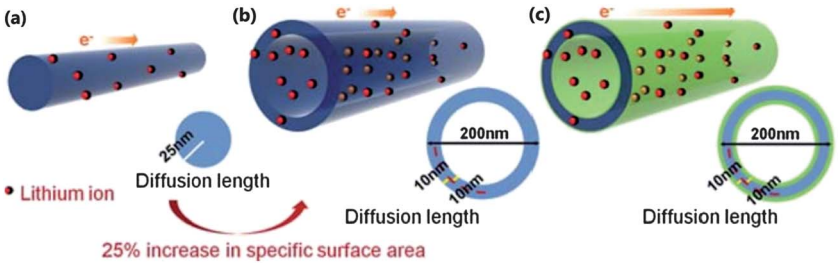

Fig. 8 The schematic diagram of (a) TiO_2 nanofibers, (b) TiO_2 hollow nanofibers and (c) nitridated TiO_2 hollow nanofibers. Reprinted with permission from Royal Society of Chemistry.[68]

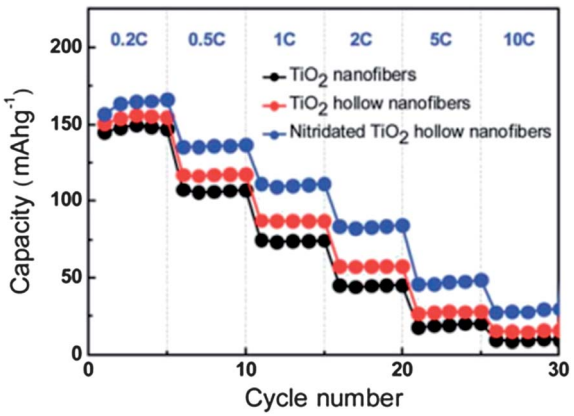

Fig. 9 The comparison of the specific capacity of TiO_2 nanofibers, TiO_2 hollow nanofibers and nitridated TiO_2 hollow nanofibers at different current densities. Reprinted with permission from Royal Society of Chemistry.[68]

Yuan *et al.*[51] modified the texture of the TiO_2 electrode based on copper foil with a silver paste, which could increase the roughness of the copper foil surface and further benefit the contact area between the electrode and the current collector as well as the adhesion of the fiber mat to the collector, Fig. 10(a). The hollow fibers were fabricated with the same $Ti(OiPr)_4$ precursor. The silver nanoparticles were also synthesized through a simple salt hydrolysis process. The copper foil was modified by coating a silver paste on the surface with a subsequent thermal treatment in an inert atmosphere to pyrolyze the organics and increase the roughness. The electrode performance has been optimized with the second discharge capacity up to 130 mA h g^{-1} at 1 C current rate and its morphology was retained perfectly even after 50 cycles, Fig. 10(b) and (c). A rougher surface of copper foil could provide more contact area between the electrode and the current collector and the rougher foil also enhanced the adhesion of the fiber film to the current collector. Therefore, the electrode performance was improved greatly.

Based on this mechanism, Park *et al.*[74] further studied hollow TiO_2 nanofibers with an inner SnO_2 layer, working as the anode for lithium ion batteries due to the high capacity of SnO_2 (about 800 mA h g^{-1}) and its fast electron transportation. Tetrabutyltin and mineral oil were mixed as the core solution. $Ti(OiPr)_4$ was dissolved in acetic acid and ethanol solvent, and further mixed with PVP–ethanol solution as the sheath material. Hollow nanofibers were obtained through an additional annealing process at 500 °C in air for 1 h. And the working electrode was fabricated by directly placing hollow nanofibers on the stainless steel foil without any conductive agent and binder. For comparison, the electrode was also prepared by mixing TiO_2 hollow nanofibers, carbon black and PVDF with a weight ratio of 80 : 10 : 10, respectively in *N*-methyl-2-pyrrolidone. The lithiation and delithiation processes are illustrated in Fig. 11. The SnO_2–TiO_2 coaxial nanofibers were also fabricated through coaxial electrospinning with the same precursor and a

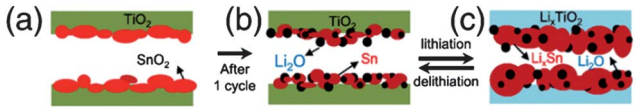

Fig. 11 (a)–(c) exhibit the morphological changes during lithiation and delithiation. Reprinted with permission from Elsevier.[74]

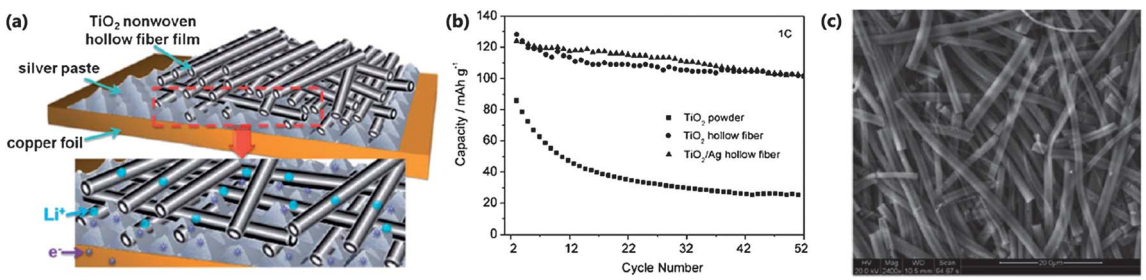

Fig. 10 (a) The schematic diagram of the TiO_2 nonwoven film on the modified copper foil with silver; (b) cycling performance of the commercial anatase TiO_2 powder as the electrode without a conductive agent, TiO_2 and TiO_2/Ag hollow fiber as the electrode with rough copper foil as the current collector and (c) SEM image of TiO_2/Ag hollow fibers after 50 cycles. Reprinted with permission from Royal Society of Chemistry.[51]

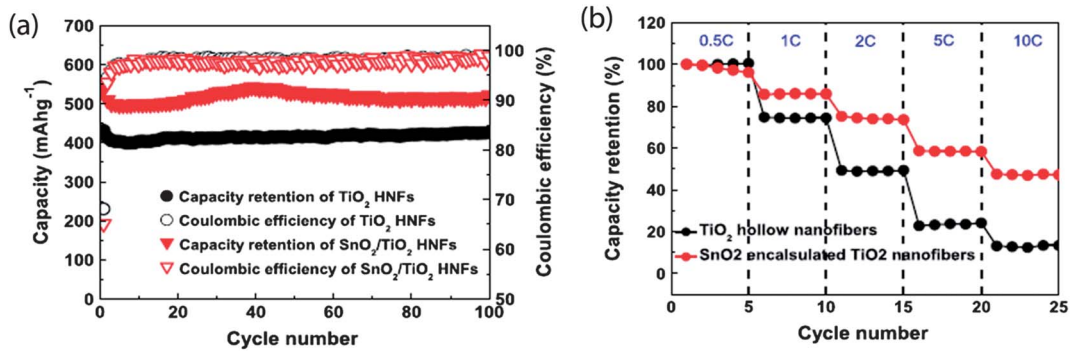

Fig. 12 Comparison of TiO_2 and SnO_2–TiO_2 hollow nanofibers, (a) cycle retentions and coulombic efficiencies, (b) rate capability at different discharge rates. Reprinted with permission from Elsevier.[74]

similar post-treatment. The hollow fibers could provide larger reaction area for the lithiation and delithiation processes. As shown, the TiO_2 hollow nanofibers with internally adhered SnO_2 nanoparticles displayed a considerably high charge and discharge capacity (517 and 802 mA h g^{-1}) at the first cycle as compared with those of the previous TiO_2 based cases. And its capacity was rather stable even after 100 cycles, Fig. 12.

2.2 Solar cells and luminescence

Other than serving as electrodes for lithium ion batteries, coaxial electrospun fibers have also been applied in other electrochemical fields, such as electrodes of solar cells and luminescence materials. Due to the non-renewability of traditional fossil energy and its environmental impact, scientists have been searching and developing clean future energy resources, among which solar, wind, nuclear and even biomass energies have been used commercially. Particularly, solar energy has attracted extensive attention due to its environmentally friendly nature, stabilization and regeneration. Furthermore, the energy that the earth receives in just one hour can support the whole energy consumption of our world in one year.[75] Thus solar energy has great potential to be developed for future deployments through conversion to electricity in solar cells. However, the charge recombination especially at the anode is a very serious problem that limits the efficiency. Different strategies have been explored to suppress the charge recombination, for example, reduced recombination sites[76] and construction of an energy barrier.[77] The core–sheath nanofibers are excellent candidates that can satisfy these two requirements. The tiny dimension could reduce the possibility that electrons recombine with the electrolyte and the sheath phase can naturally prevent serious combination as barriers. On the other hand, light is a very common, but very potential future energy. There are two ways to generate light, incandescence and luminescence.[78] Incandescence describes that items such as tungsten filament can emit light when heated to a very high temperature. Compared with incandescence, luminescence refers to "cool light", such as the screens of electronic devices. Luminescence is caused by the jump of excited electrons back to the less excited or ground state. The energy difference is released in the form of "cool light". Luminescence can be classified into many different types according to input energy sources, such as chemiluminescence, electroluminescence, triboluminescence and bioluminescence. If the input energy is another kind of light, for example, ultraviolet radiation or X-ray, this luminescence is called fluorescence. Many materials have been found to be luminescent, including transition metal ions, rare earth metal complexes, heavy metals, quartz, feldspar and aluminum oxide with electron–hole pairs. Some organic materials are also luminescent. Luminescence makes materials detectable and scientists are trying to develop new signaling systems and devices with luminescent materials[79] aiming to fabricate sensors with high efficiency and accuracy in detection, biological and medicine engineering.[80–82] New luminescent materials have been prepared for light-emitting diodes (LEDs), which have longer service time, lower energy consumption and stronger brightness.[83–85] The utilization of core–sheath nanofibers could increase the contact area, which is beneficial for the excitation process. On the other hand, the fiber form can integrate optical and optoelectronic devices into textile.[86]

For example, Du *et al.*[87] have fabricated a TiO_2–Nb_2O_5 core–sheath nanofiber film. $Ti(OiPr)_4$, PVA and HAc DMF solution served as the TiO_2 precursor. $C_{10}H_{25}NbO_5$ and PVA DMF solution served as the Nb_2O_5 precursor. The as-spun fibers were calcined at 500 °C for 1 h with a heating rate of 1 °C min^{-1} and then cooled naturally. After calcination, the fibers become more curved and rougher. The fiber film worked as a photoanode in the dye-sensitized solar cells. Its working mechanism is shown in Fig. 13. The bandgap of Nb_2O_5 is 3.5 eV, while that of TiO_2 is 3.2 eV and the conduction band (E_{cb}) of Nb_2O_5 is 0.25 eV higher than that of TiO_2.[88] The bandgap difference will cause the

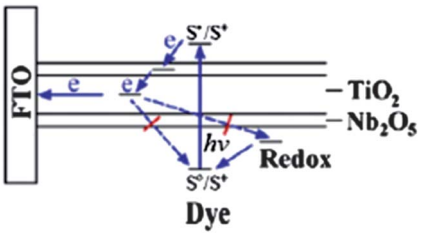

Fig. 13 Schematic diagram of the catalyst mechanism of the TiO_2–Nb_2O_5 core–sheath structure. Reprinted with permission from Elsevier.[87]

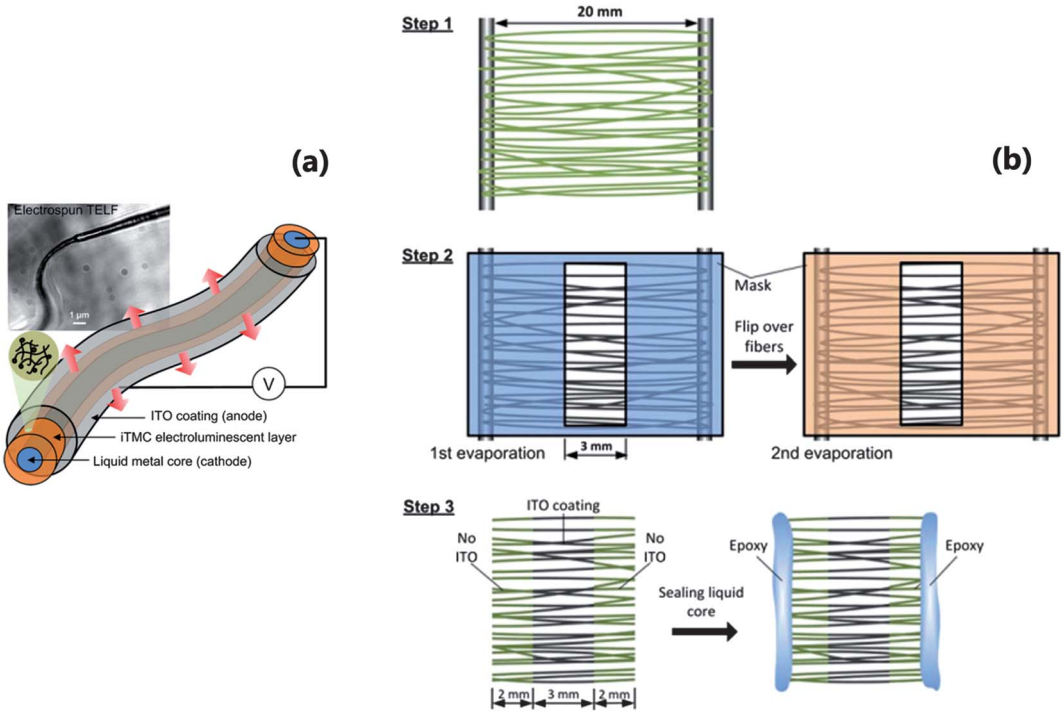

Fig. 14 (a) The texture schematic diagram and TEM image and (b) schematic for fabrication procedures of TELFs. Reprinted with permission from American Chemical Society.[86]

charge equilibrium and energy system to be rearranged between the core–sheath structures. And a higher charge transport resistance at the anode–electrolyte interface will be formed, which could form an energy barrier and restrain the charge recombination. Therefore, the energy conversion efficiency (η), which is the ratio of the converted photoenergy to the incident light intensity, increases from 4.5 up to 5.8%.

Yang *et al.*[86] have reported a novel application of coaxial electrospun core–sheath fibers. Combining the electrospun core–sheath structure and indium-tin oxide (ITO) plating deposition, three coaxial layers have been integrated into one single fiber, Fig. 14(a). The core was a highly conductive metal alloy liquid phase, consisting of 68.5 wt% Ga, 21.5 wt% In and 10 wt% Sn. The sheath phase was the mixture of ruthenium(II)

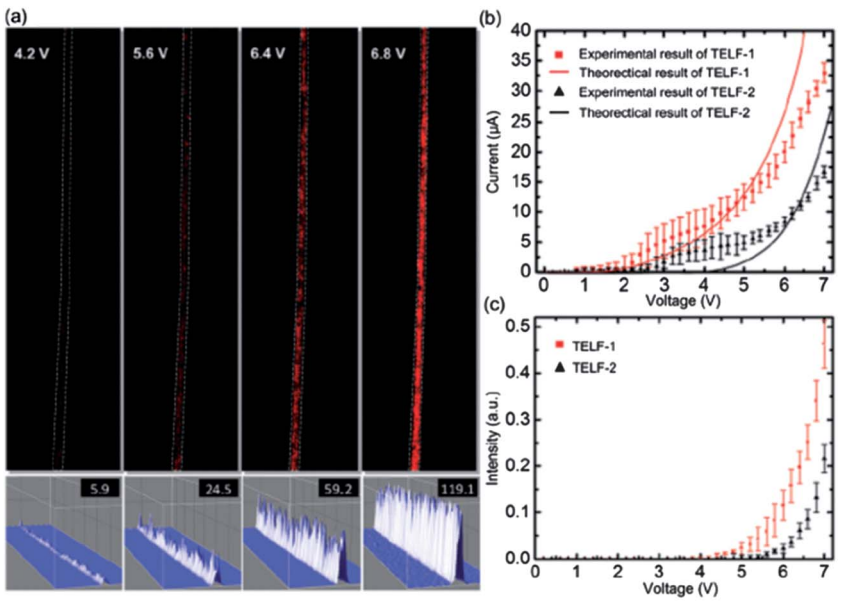

Fig. 15 (a) Luminescence responses of TELF-1 to different voltages applied to the device in N_2. (b) Experimental and theoretical results for current–voltage characteristics of TELF-1 and TELF-2. (c) Experimental results for current–luminance characteristics of TELF-1 and TELF-2. Reprinted with permission from American Chemical Society.[86]

tris(bipyridine) $[Ru(bpy)_3]^{2+}[(PF6)^-]_2$ and PEO. And the inner sheath phase was an ionic transition-metal complex (iTMC). For comparison, TELF-1 and TELF-2, fibers with different dimensions were fabricated by adjusting the flow rate of core and sheath phases. Specifically, core and sheath flow rates were 0.13 and 0.25 mL h^{-1} for TELF-1 and 0.15 and 0.31 mL h^{-1} for TELF-2. After coaxial electrospinning, the obtained core–sheath fibers were deposited on an ITO thin film on the surface, Fig. 14(b). Only the central portion (3 mm) of the fibers was exposed to vapor for deposition and the remaining part was marked, step 2. After deposition, 7 mm long fibers were cut and sealed with epoxy at the edge to prevent the leakage of liquid metal. And the three layered nanofibers were formed. Interestingly, the core phase and the outer sheath phase acted as an anode and a cathode, respectively and the electrolyte ($[Ru(bpy)_3]^{2+}[(PF6)^-]_2$ and PEO) was the electroluminescent layer. TELFs were placed on the stage of an inverted microscope in a dark room. A customized electronic probe station with a gold coated AFM tip was attached to the microscope. To make an electrical contact, the tip was pressed to poke through the polymer shell. And light emitted from the device was collected by using a QICAM color camera. When an external voltage was applied, charge could be transported in the lighting device. Emissive charge carriers were driven into the iTMC layer from the electrode and the recombination occurred along with the release of energy in the light form. As shown in Fig. 15(a), the CCD camera began to capture visible red light at 4.2 V, which was called the turn-on voltage and the light could be distinguished by eyes at 5.6 V in N_2. And the luminance from coaxial nanofibers became stronger with the increasing applied voltage, because more charge carriers would be transported into the iTMC layer under stronger potential difference, and more energy would release from the combination. And the current–voltage and luminance intensity–voltage characteristics are illustrated in Fig. 15(b) and (c). There always was a turn-on voltage for both samples to generate current and emit light. TELF-1 exhibited more sensitivity to the voltage, because a stronger electrical field was formed in thinner fibers at certain voltage values. And the current value experienced a fluctuation and then followed a potential trend. This was due to the redistribution of $PF6^-$ and different injection manners at different voltage values. This technique is very meaningful in many research fields such as bioimaging and sensing.

2.3 Supercapacitors

A capacitor is a kind of significant energy storage device due to its high power density. Generally, a capacitor is constructed by two parallel conducting plates separated by some solid dielectrics or even air. When an external potential difference is applied, charges cannot pass through the capacitor due to the presence of a dielectric, and they will accumulate on the corresponding plate and the energy is thus stored. Its disadvantage is the low energy density compared with a battery. So a supercapacitor comes out possessing high energy and power density. The plate and dielectric materials of a supercapacitor are improved. Researchers use electrolytes instead of conventional solid dielectrics. So opposite ions will accumulate around the charged electrode and form the electric double layer. The input energy is stored here and this type of capacitor is called an electric double-layer capacitor (EDLC). Another type of supercapacitor is called a pseudocapacitor. When getting charged, ions can react with the electrode material and the stored chemical energy can be fast released through some redox reactions.[89,90]

A capacitor has its special characteristic, capacitance, which is the ratio of accumulated charges on one plate to potential difference between two plates. Experimentally, the capacitance can be evaluated through cyclic voltammetry and galvanostatic charge–discharge methods.[91,92] In the cyclic voltammetry method, the input and output voltage rate is controlled at a certain fixed value and the current is recorded. And the capacitance (C_s, F g^{-1}) is calculated from eqn (1).

$$C_s = \frac{\int i dV}{2m \cdot \Delta V \cdot S} \quad (1)$$

where $\int idV$ is the integrated area of the CV curve, m is the mass of electrode active materials in g, ΔV is the scanned potential range in V and S is the scan rate in V s^{-1}. The galvanostatic method is very similar, in which the controlled parameter is the current and the voltage value is recorded. And the capacitance (C_s, F g^{-1}) is calculated from eqn (2).

$$C_s = \frac{i \times \Delta t}{m \times \Delta V} \quad (2)$$

where i is the discharge current in A, Δt is the discharge time in s, m is the mass of electrode active materials in g, and ΔV is the potential drop during discharge in V.

To date, supercapacitors have been developed as a significant alternative energy storage unit[93–95] due to their high power and energy density, rapid charge–discharge capacity and long life time.[7,96] Different materials have been explored to fabricate supercapacitors with improved electrochemical performances. Generally, metal oxides and conducting polymers are used as electrode materials. For example, ruthenium oxide, a transition metal oxide, possesses a large electrochemical capacitance, 150–260 F cm^{-2}, which is ten times higher than that of carbon and provides a facile pathway for the transportation of both protons and electrons, however, there are abundant boundaries in its nanostructures, which resist the charge transfer.[97,98] Polyaniline and polypyrrole have excellent conductivity, high pseudo-capacitance and low cost,[99–102] but their mechanical stability is not strong enough during the repetitive charging–discharging process for electrochemical energy storage.[103] Therefore, scientists have used various inorganic fillers such as silica,[104] carbon nanutubes,[105] and graphite oxide[106] to form composites, which have demonstrated an endured electrochemical energy storage performance and high capacitance in the thin film structures.

Nanomaterial is a suitable choice due to its high specific surface area, which is beneficial for the contact between electrode and electrolyte. Scientists have integrated different materials to fabricate heterogeneous composites with tiny dimensions to achieve high capacitance and stability. Core–sheath nanofibers with extremely tiny dimensions and heterogeneous self-supporting structures are potential materials for

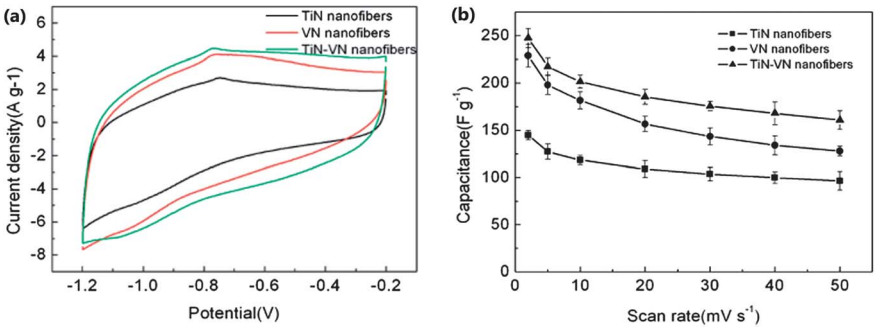

Fig. 16 (a) CV curve of TiN, VN and TiN–VN fibers cycled between −1.2 and −0.2 V at a sweep rate of 20 mV s^{-1}; (b) specific capacitances of the electrodes with TiN, VN and TiN–VN fibers respectively at progressive scan rates from 2 to 50 mV s^{-1}. Reprinted with permission from American Chemical Society.[107]

supercapacitors. For example, Zhou *et al.*[107] have fabricated mesoporous titanium nitride (TiN)–vanadium nitride (VN) core–sheath fibers and studied the supercapacitor performance. TiN displays a good electrical conductivity, but its capacity is poor. While VN has a higher capacity, it has a poor conductivity. The integration of these two materials could achieve a better performance. In the experiment, $Ti(OBu)_4$ and $V(C_5H_7O_2)_3$ were used as the precursors of TiN and VN and dissolved into isopropyl alcohol and the mixture of ethylene glycol and absolute ethanol, respectively. PVP was added to both solutions as a stabilizer. The as-spun fibers were dried for 2–4 h at 50 °C to remove solvents. An additional thermal treatment was carried out at 800 °C in an ammonia atmosphere for 1 h with a slow heating rate (room temperature to 300 °C, 5 °C min^{-1}; 300 to 700 °C, 2 °C min^{-1} and 700 to 800 °C, 1 °C min^{-1}). Mesoporous fibers were obtained. And both precursor sols were electrospun respectively, following the same post-treatment for comparison. The working electrode was prepared by mixing nanofibers with carbon blacks and polytetrafluoroethylene (PTFE) binders with a weight ratio of 85 : 5 : 10. And the samples were cut into plates of 0.5 cm × 0.5 cm and then pasted on a stainless steel current collector under 15 MPa pressure. The electrochemical property was studied with a three-electrode system. As shown in Fig. 16(a), the capacity of TiN–VN (185 F g^{-1}) is clearly higher than the other two (109 F g^{-1} for TiN and 157 F g^{-1} for VN). The overall specific capacitances of the three samples at different scan rates have been tested and that of TiN–VN was much more desirable under various conditions. In Fig. 16(b), the TiN sample exhibited better capacitance retention especially at a high scan rate. The VN sample possessed a higher capacitance, but poor rate capability. And TiN–VN integrated the two merits: excellent capacity and stability. By increasing the scan rate and current density of the TiN–VN sample, the capacitance decreases by different degrees.

2.4 Photocatalytic environmental remediation

Nanomaterials have served as catalysts due to their high surface area to volume ratio and high specific catalytic activity.[108,109] Among these catalytic nanostructures, the core–sheath or hollow nanofibers exhibit much better adaptability for a wide range of applications, such as new energy and environmental protection.[110] The core–sheath structure could bring many benefits, such as decreased diffusion length, increased accessible surface area and more active sites, all of which can improve the photocatalyst activity. And the hollow fibers encapsulated with nanoparticles could experience an efficient charge transportation, which also favors the photocatalytic process.[111]

TiO_2 is a very popular semiconductor used as a photocatalyst due to its facile functionality, stability, nontoxicity and low cost, however, its high energy gap (3.2 eV) and high rate of recombination of the electron–hole pair limit its performance.[112,113] Meanwhile, some components including noble metals,[114] transition metals[115] and nonmetals[116] have been doped to prevent the

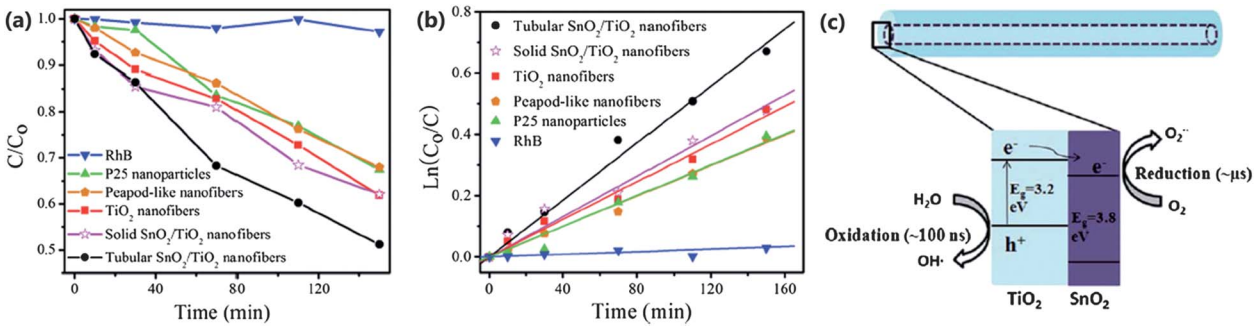

Fig. 17 (a) Degradation profiles of Rhodamine B with different photocatalysts under UV illumination; (b) the pseudo first-order kinetic relationship with different photocatalysts; (c) the configuration of the energy band of core–sheath fibers and the charge separation at the interface of SnO_2 and TiO_2. Reprinted with permission from Royal Society of Chemistry.[111]

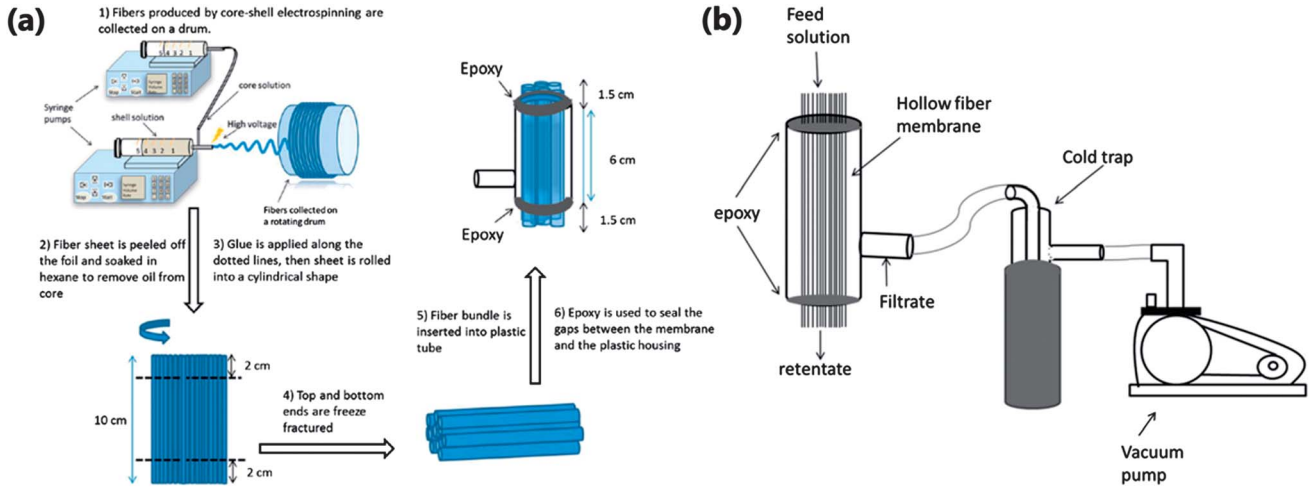

Fig. 18 The schematic diagram of the hollow fiber membrane filtration setup. Reprinted with permission from American Chemical Society.[40]

recombination of charge carriers and to enhance its response to visible light. For example, Peng *et al.*[111] have selected SnO_2 to dope TiO_2 to increase its photocatalytic performance. Briefly, titanium isopropoxide ($Ti(OiPr)_4$) and tin ethylhexanoate ($C_{16}H_{30}O_4Sn$) were used as the TiO_2 and SnO_2 precursors, respectively. After electrospinning, the obtained fibers were naturally dried for one day to complete the hydrolysis of $Ti(OiPr)_4$ and calcined in air at 500 °C for 2 h to allow the formation of SnO_2 nanoparticles. The obtained fibers possess a highly uniform coaxial heterogeneous structure. Interestingly, with increased concentration of the tin precursor in core solution, the final texture of the electrospun fibers could be tuned from hollow tubes to "peapod" filled fibers and further to solid core–sheath fibers.[111] Though the bandgap (3.8 eV) of SnO_2 is higher than that of TiO_2, its conduction band is lower than that of TiO_2. Therefore, electrons can easily migrate from TiO_2 to the conduction band of SnO_2, which will leave photogenerated holes in the valence band of TiO_2 and accumulate lots of electrons in the SnO_2 phase. This will facilitate the photogenerated charge separation, improve the photocatalytic performance and shift the photoexcitation of samples to visible light.[117,118] In the photocatalytic activity tests, the relative concentrations of Rhodamine B at different times were plotted and the experimental data were fitted to follow a pseudo-first-order reaction model. The tubular core–sheath SnO_2–TiO_2 fibers were observed to display the best photocatalytic performance with the highest reaction rate constant compared to other samples, Fig. 17. This enhanced photocatalytic behaviors (with an higher efficiency about 1.4 times of solid SnO_2–TiO_2 and 1.8 times of commercial TiO_2 nanoparticles) are attributed to the core–sheath structure of the fibers as well as the energy level offset between SnO_2 and TiO_2. On the other hand, the electron transfer from TiO_2 to SnO_2 will suppress the recombination of the charge carriers.

2.5 Filtration

Nanofibers are a perfect choice for different types of separation, such as air purification, solution filtration and osmosis separation, due to their extremely high surface area to volume ratio,

Table 1 Parts of the composition of core–sheath solution pairs

	Core phase		Sheath phase		
No.	Solute	Solvent	Solute	Solvent	Ref.
1	PVP	Ethanol	PVP	DMAc	30
2	PEO	Acetic acid aqueous solution	Chitosan	Acetic acid aqueous solution	31
3	—	Mineral oil	$Ti(OiPr)_4$ and PVP	Acetic acid and ethanol	68
4	Tetrabutyltin	Mineral oil	$Ti(OiPr)_4$ and PVP	Acetic acid and ethanol	74
5	$Ti(OiPr)_4$, PVA	Acetic acid, DMF	$C_{10}H_{25}NbO_5$, PVA	DMF	87
6	Nanosilver	Mineral oil	$Ti(OiPr)_4$, PVP	Acetic acid and ethanol	51
7	Tin ethyl hexanoate	Light mineral oil	$Ti(OiPr)_4$, PVP	Ethanol	111
8	Cellulose acetate and ketoprofen	Acetone, ethanol and DMAc	—	Acetone, ethanol and DMAc	25
9	Styrene-*co*-acrylonitrile	DMF	PAN	DMF	63
10	PVA	DMSO and ethanol	PVDF	DMSO and acetone	45
11	SAN	DMF	PAN	DMF	42
12	PVP	Ethanol	Sodium chloride	H_2O	39
13	PEG	H_2O	PLLA	DCM and DMF	32
14	—	Mineral oil	PAN	DMF	40
15	—	Mineral oil	PAN	DMF	72
16	PEG and protein	H_2O	PCL	Chloroform and DMF	26

highly porous structure and chemical properties in some special cases, as well as the flexibility and low cost. And there are already some review papers discussing on this topic.[119,120] Generally, the electrospun nanofiber mats can be used for filtration directly. And some researchers have used fibers for waste water purification.[121,122] The unique structure of hollow nanofibers becomes the intrinsic advantage as the osmosis membrane material. And the appropriate selection of sheath material could promise better performance in separation. Since the convenient fabrication of hollow fibers through the coaxial electrospinning process, it has opened a new door to this field. Anka *et al.*[40] have reported the wonderful separation performance of the PAN hollow fiber membrane upon treatment with Indigo carmine dye and sodium chloride solutions. They used PAN–DMF solution as the sheath and mineral oil as the core. And the as-spun fibers were sunk into hexane to remove the core phase. The fabrication and filtration processes are illustrated in Fig. 18(a) and (b). The results showed that the dye and sodium salt were rejected 100 and 97.7% $\pm$ 0.6, respectively.

3 Component list

Here, the compositions of core–sheath solution pairs are summarized in Table 1.

4 Conclusions and perspectives

As an innovation of conventional electrospinning, coaxial electrospinning has attracted much attention and has been studied deeply. The parameters, including both the internal physical properties and the external operation factors have been analyzed theoretically and experimentally. In particular, the interaction between different phases due to the contact and the heterogeneousness, which is also the characteristic of coaxial electrospinning, is discussed in detail. The evaporation rate, polymer concentration, conductivity and flow rate have been systematically reviewed in achieving smooth and uniform morphology as well as fine dimension. Generally, a stronger and longer electrospinning process can result in more smooth fibers. All strategies to enhance the electrical force and elongate the electrospinning whipping stage will favor the final fibers. However, there will always be a suitable operation range for all parameters, only within which non-beaded fibers can be obtained. The lower limitation is the critical value, beyond which the electrospinning process can take place. And the higher limitation can prevent the strong effect on the formation of core–sheath fibers. The interaction due to the property difference should promise the formation of the core–sheath Taylor cone and the smooth electrospinning process. Too huge a difference may lead to a significantly different behavior during electrospinning. Through additional treatment, hollow nanofibers can be fabricated. The following extraction process or thermal treatment can remove the core phase, maintaining the complete sheath structure. In addition, the thermal treatment is much quicker and can stabilize and carbonize the polymer matrix at the same time, which can increase its efficiency.

Nearly all polymer solutions and their polymer composite matrices could be fabricated into core–sheath and hollow nanofibers through the coaxial electrospinning technique. Through appropriate post-treatments of the electrospun fibers, various inorganic nanofibers or nanotubes have been developed with much wider applications including photocatalysis, lithium ion batteries, supercapacitors, solar cells, *etc.* The obtained nanofibers possess extremely high specific surface area and combined properties, which have shown superior performance over the traditional electrospun fibers.

However, there are also some challenges, such as the dimension and order of the obtained nanofibers, the improved performance in their applications and the expanded applications of the core–sheath and hollow nanofibers. So far, the fine dimension of the core–sheath nanofibers is about 60 nm, which is much larger than that of the fibers through conventional electrospinning, about a few nanometers. The obtained fibers are in random order, not aligned. To obtain ultra-fine core–sheath nanofibers, the matrices should be selected properly for both phases, as well as the operation parameters, collection method and post-treatment methods, such as thermal treatment. To develop the properties and performance of core–sheath and hollow nanofibers, new materials should be tested to integrate into both phases as desired, for example, biomaterials can be used as the matrix to increase the biocompatibility in applications of tissue engineering. Polymers can be integrated into a sheath phase to fabricate high strength materials with very low density. Different nanoparticles can be loaded to achieve suitable interactions during charging and discharging processes and catalysis.

Core–sheath and hollow nanofibers are very promising potential materials in various applications due to their flexibility and excellent physicochemical properties. Therefore, more amazing and meaningful applications of the materials are envisioned to be achieved in the future when deployed in other fields, such as the magnetic nanocomposites, semiconductors, carbon materials with high strength and conductivity, anticorrosion and fire-proof properties.

Acknowledgements

The authors appreciate the support from the Research Enhancement Grant (REG) of Lamar University. Partial financial support from NSF-Nanomanufacturing (CMMI-13-14486), Nanoscale Interdisciplinary Research Team and Materials Processing and Manufacturing (CMMI 10-30755) and Chemical and Biological Separations (CBET 11-37441) is acknowledged.

References

1 N. Phong, M. Gabr, K. Okubo, B. Chuong and T. Fujii, *Compos. Struct.*, 2013, **99**, 380–387.
2 C. Huang, S. Chen, C. Lai, D. H. Reneker, H. Qiu, Y. Ye and H. Hou, *Nanotechnology*, 2006, **17**, 1558.
3 Y. Zhou, M. Freitag, J. Hone, C. Staii, A. Johnson, N. J. Pinto and A. MacDiarmid, *Appl. Phys. Lett.*, 2003, **83**, 3800–3802.

4 J. Zhao, Y. Cheng, X. Yan, D. Sun, F. Zhu and Q. Xue, *CrystEngComm*, 2012, **14**, 5879–5885.
5 L. Lang, D. Wu and Z. Xu, *Chem.–Eur. J.*, 2012, **18**, 10661–10668.
6 D. Han, S. T. Boyce and A. J. Steckl, *Mater. Res. Soc. Symp. Proc.*, 2008, **1094**, 1–6.
7 J. Miao, M. Miyauchi, T. J. Simmons, J. S. Dordick and R. J. Linhardt, *J. Nanosci. Nanotechnol.*, 2010, **10**, 5507–5519.
8 M. Miyauchi, J. Miao, T. J. Simmons, J.-W. Lee, T. V. Doherty, J. S. Dordick and R. J. Linhardt, *Biomacromolecules*, 2010, **11**, 2440–2445.
9 N. E. Zander, *Polymers*, 2013, **5**, 19–44.
10 H. Zhang, C. Zhao, Y. Zhao, G. Tang and X. Yuan, *Sci. China: Chem.*, 2010, **53**, 1246–1254.
11 I. G. Loscertales, A. Barrero, M. Márquez, R. Spretz, R. Velarde-Ortiz and G. Larsen, *J. Am. Chem. Soc.*, 2004, **126**, 5376–5377.
12 N. E. Zander, K. E. Strawhecker, J. A. Orlicki, A. M. Rawlett and T. P. Beebe, *J. Phys. Chem. B*, 2011, **115**, 12441–12447.
13 G. Fu, J. Lei, C. Yao, X. Li, F. Yao, S. Nie, E. Kang and K. Neoh, *Macromolecules*, 2008, **41**, 6854–6858.
14 J.-G. Wang, Y. Yang, Z.-H. Huang and F. Kang, *Electrochim. Acta*, 2011, **56**, 9240–9247.
15 Y. Yang, H. Wang, X. Lu, Y. Zhao, X. Li and C. Wang, *Mater. Sci. Eng., B*, 2007, **140**, 48–52.
16 Y. Dror, W. Salalha, R. Avrahami, E. Zussman, A. L. Yarin, R. Dersch, A. Greiner and J. H. Wendorff, *Small*, 2007, **3**, 1064–1073.
17 O. S. Kwon, E. Park, O. Y. Kweon, S. J. Park and J. Jang, *Talanta*, 2010, **82**, 1338–1343.
18 J.-F. Zhang, D.-Z. Yang, F. Xu, Z.-P. Zhang, R.-X. Yin and J. Nie, *Macromolecules*, 2009, **42**, 5278–5284.
19 Y. Yang, X. Li, W. Cui, S. Zhou, R. Tan and C. Wang, *J. Biomed. Mater. Res., Part A*, 2008, **86**, 374–385.
20 X. Li, H. Zhang, H. Li and X. Yuan, *Colloid Polym. Sci.*, 2010, **288**, 1113–1119.
21 H. Xiang, Y. Long, X. Yu, X. Zhang, N. Zhao and J. Xu, *CrystEngComm*, 2011, **13**, 4856–4860.
22 G. Dong, X. Xiao, M. Peng, Z. Ma, S. Ye, D. Chen, H. Qin, G. Deng, Q. Liang and J. Qiu, *RSC Adv.*, 2012, **2**, 2773–2782.
23 Y. Cheng, B. Zou, C. Wang, Y. Liu, X. Fan, L. Zhu, Y. Wang, H. Ma and X. Cao, *CrystEngComm*, 2011, **13**, 2863–2870.
24 I. G. Loscertales, A. Barrero, I. Guerrero, R. Cortijo, M. Marquez and A. M. Gañán-Calvo, *Science*, 2002, **295**, 1695–1698.
25 D. Yu, J.-H. Yu, L. Chen, G. R. Williams and X. Wang, *Carbohydr. Polym.*, 2012, **90**, 1016–1023.
26 H. Jiang, Y. Hu, Y. Li, P. Zhao, K. Zhu and W. Chen, *J. Controlled Release*, 2005, **108**, 237–243.
27 Y. Zhang, Z.-M. Huang, X. Xu, C. T. Lim and S. Ramakrishna, *Chem. Mater.*, 2004, **16**, 3406–3409.
28 J. H. Yu, S. V. Fridrikh and G. C. Rutledge, *Adv. Mater.*, 2004, **16**, 1562–1566.
29 Z. Sun, E. Zussman, A. Yarin, J. Wendorff and A. Greiner, *Adv. Mater.*, 2003, **15**, 1929–1932.
30 D. Yu, C. Branford-White, K. White, N. Chatterton, L. Zhu, L. Huang and B. Wang, *eXPRESS Polym. Lett.*, 2011, **5**, 732–741.
31 M. Pakravan, M.-C. Heuzey and A. Ajji, *Biomacromolecules*, 2012, **13**, 412–421.
32 K.-L. Ou, C.-S. Chen, L.-H. Lin, J.-C. Lu, Y.-C. Shu, W.-C. Tseng, J.-C. Yang, S.-Y. Lee and C.-C. Chen, *Eur. Polym. J.*, 2011, **47**, 882–892.
33 Y. Z. Zhang, X. Wang, Y. Feng, J. Li, C. T. Lim and S. Ramakrishna, *Biomacromolecules*, 2006, **7**, 1049–1057.
34 J. Díaz, A. Barrero, M. Márquez and I. Loscertales, *Adv. Funct. Mater.*, 2006, **16**, 2110–2116.
35 S. Chakraborty, I. Liao, A. Adler and K. W. Leong, *Adv. Drug Delivery Rev.*, 2009, **61**, 1043–1054.
36 Y. Hang, Y. Zhang, Y. Jin, H. Shao and X. Hu, *Int. J. Biol. Macromol.*, 2012, **51**, 980–986.
37 A. K. Moghe and B. S. Gupta, *Polym. Rev.*, 2008, **48**, 353–377.
38 A. K. Moghe, *Core–sheath Differentially Biodegradable Nanofiber Structures for Tissue Engineering*, ProQuest, Ann Arbor, 2008.
39 D. Yu, K. White, J. Yang, X. Wang, W. qian and Y. Li, *Mater. Lett.*, 2012, **67**, 78–80.
40 F. H. Anka and K. J. Balkus, *Ind. Eng. Chem. Res.*, 2013, **52**, 3473–3480.
41 A. L. Yarin, E. Zussman, J. Wendorff and A. Greiner, *J. Mater. Chem.*, 2007, **17**, 2585–2599.
42 B.-S. Lee, S.-B. Son, K.-M. Park, J.-H. Seo, S.-H. Lee, I.-S. Choi, K.-H. Oh and W.-R. Yu, *J. Power Sources*, 2012, **206**, 267–273.
43 D. Li and Y. Xia, *Nano Lett.*, 2004, **4**, 933–938.
44 Y. Chen, Z. Lu, L. Zhou, Y.-W. Mai and H. Huang, *Energy Environ. Sci.*, 2012, **5**, 7898–7902.
45 H. Na, P. Chen, S.-C. Wong, S. Hague and Q. Li, *Polymer*, 2012, **53**, 2736–2743.
46 P. Zhao, H. Jiang, H. Pan, K. Zhu and W. Chen, *J. Biomed. Mater. Res., Part A*, 2007, **83**, 372–382.
47 F. Li, Y. Zhao and Y. Song, *Nanofibers*, InTech, 2010, ISBN: 978-953-7619-86-22010.
48 M. Kamperman, L. T. Korley, B. Yau, K. M. Johansen, Y. L. Joo and U. Wiesner, *Polym. Chem.*, 2010, **1**, 1001–1004.
49 Q. Xu, N. Zhang, W. Qin, J. Liu, Z. Jia and H. Liu, *J. Nanosci. Nanotechnol.*, 2013, **13**, 149–156.
50 Z. Kurban, A. Lovell, S. M. Bennington, D. W. K. Jenkins, K. R. Ryan, M. O. Jones, N. T. Skipper and W. I. F. David, *J. Phys. Chem. C*, 2010, **114**, 21201–21213.
51 T. Yuan, B. Zhao, R. Cai, Y. Zhou and Z. Shao, *J. Mater. Chem.*, 2011, **21**, 15041–15048.
52 Y. Su, X. Li, H. Wang, C. He and X. Mo, *J. Mater. Sci.: Mater. Med.*, 2009, **20**, 2285–2294.
53 C. Wang, K. Yan, Y. Lin and P. Hsieh, *Macromolecules*, 2010, **43**, 6389–6397.
54 A. L. Yarin, *Polym. Adv. Technol.*, 2011, **22**, 310–317.
55 W.-J. Zhang, *J. Power Sources*, 2011, **196**, 13–24.
56 P. Verma, P. Maire and P. Novák, *Electrochim. Acta*, 2010, **55**, 6332–6341.
57 S. Al-Thyabat, T. Nakamura, E. Shibata and A. Iizuka, *Miner. Eng.*, 2013, **45**, 4–17.
58 M. Song, S. Park, F. Alamgir, J. Cho and M. Liu, *Mater. Sci. Eng., R*, 2011, **72**, 203–252.

59 V. Etacheri, R. Marom, R. Elazari, G. Salitra and D. Aurbach, *Energy Environ. Sci.*, 2011, **4**, 3243–3262.
60 H. Yan, Z. Zhu, D. Zhang, W. Li and A. M. Qilu, *J. Power Sources*, 2012, **219**, 45–51.
61 B. Peng and J. Chen, *Coord. Chem. Rev.*, 2009, **253**, 2805–2813.
62 Y. P. Wu, E. Rahm and R. Holze, *J. Power Sources*, 2003, **114**, 228–236.
63 B.-S. Lee, S.-B. Son, K.-M. Park, W.-R. Yu, K.-H. Oh and S.-H. Lee, *J. Power Sources*, 2012, **199**, 53–60.
64 X. Xiao, P. Liu, M. W. Verbrugge, H. Haftbaradaran and H. Gao, *J. Power Sources*, 2011, **196**, 1409–1416.
65 J. Guo, A. Sun, X. Chen, C. Wang and A. Manivannan, *Electrochim. Acta*, 2011, **56**, 3981–3987.
66 S. Huang and T. Zhu, *J. Power Sources*, 2011, **196**, 3664–3668.
67 D. Cai, D. Li, S. Wang, X. Zhu, W. Yang, S. Zhang and H. Wang, *J. Alloys Compd.*, 2013, **561**, 54–58.
68 H. Han, T. Song, J.-Y. Bae, L. F. Nazar, H. Kim and U. Paik, *Energy Environ. Sci.*, 2011, **4**, 4532–4536.
69 C. Lai, G. R. Li, Y. Y. Dou and X. P. Gao, *Electrochim. Acta*, 2010, **55**, 4567–4572.
70 Z. Du, X. Yin, M. Zhang, Q. Hao, Y. Wang and T. Wang, *Mater. Lett.*, 2010, **64**, 2076–2079.
71 C. Zhu, M. Zhang, Y. Qiao, P. Gao and Y. Chen, *Mater. Res. Bull.*, 2010, **45**, 437–441.
72 B. Liu, Y. Yu, J. Chang, X. Yang, D. Wu and X. Yang, *Electrochem. Commun.*, 2011, **13**, 558–561.
73 T. Hwang, Y. Lee, B.-S. Kong, J.-S. Seo and J. W. Choi, *Nano Lett.*, 2011, **12**, 802–807.
74 H. Park, T. Song, H. Han, A. Devadoss, J. Yuh, C. Choi and U. Paik, *Electrochem. Commun.*, 2012, **22**, 81–84.
75 O. Mahian, A. Kianifar, S. A. Kalogirou, I. Pop and S. Wongwises, *Int. J. Heat Mass Transfer*, 2013, **57**, 582–594.
76 S. Ueno and S. Fujihara, *Electrochim. Acta*, 2011, **56**, 2906–2913.
77 L. Grinis, S. Kotlyar, S. Rühle, J. Grinblat and A. Zaban, *Adv. Funct. Mater.*, 2010, **20**, 282–288.
78 N. Kalyani and S. J. Dhoble, *Renewable Sustainable Energy Rev.*, 2012, **16**, 2696–2723.
79 T. Gunnlaugsson, M. Glynn, G. M. Tocci, P. E. Kruger and F. M. Pfeffer, *Coord. Chem. Rev.*, 2006, **250**, 3094–3117.
80 W. Li, W. Li, Y. Hu, Y. Xia, Q. Shen, Z. Nie, Y. Huang and S. Yao, *Biosens. Bioelectron.*, 2013, **47**, 345–349.
81 A. V. S. Lourenço, C. A. Kodaira, E. M. Ramos-Sanchez, M. C. F. C. Felinto, H. Goto, M. Gidlund, O. L. Malta and H. F. Brito, *J. Inorg. Biochem.*, 2013, **123**, 11–17.
82 Z. Li, J. Ma, Y. Zong and Y. Men, *J. Alloys Compd.*, 2013, **559**, 39–44.
83 Z. Wang, P. Li, T. Li, X. Zhang, Q. Li, Z. Yang and Q. Guo, *Mater. Res. Bull.*, 2013, **48**, 2393–2395.
84 C. Li, H. Chen, Y. Hua, L. Yu, Q. Jiang, D. Deng, S. Zhao, H. Ma and S. Xu, *Opt. Commun.*, 2013, **295**, 129–133.
85 D. Li, X. Liu, G. Xie and X. Liu, *Colloids Surf., A*, 2013, **424**, 33–39.
86 H. Yang, C. R. Lightner and L. Dong, *ACS Nano*, 2011, **6**, 622–628.
87 P. Du, L. Song, J. Xiong, Y. Yuan, L. Wang, Z. Xi, D. Jin and J. Chen, *Electrochem. Commun.*, 2012, **25**, 46–49.
88 P. Guo and M. A. Aegerter, *Thin Solid Films*, 1999, **351**, 290–294.
89 G. A. Snook, P. Kao and A. S. Best, *J. Power Sources*, 2011, **196**, 1–12.
90 T. Zhao, H. Jiang and J. Ma, *J. Power Sources*, 2011, **196**, 860–864.
91 J. Zhu, M. Chen, H. Qu, Z. Luo, S. Wu, H. A. Colorado, S. Wei and Z. Guo, *Energy Environ. Sci.*, 2013, **6**, 194–204.
92 J. Zhu, M. Chen, N. Yerra, N. Haldolaarachchige, S. Pallavkar, Z. Luo, T. C. Ho, J. Hopper, D. P. Young, S. Wei and Z. Guo, *Nanoscale*, 2013, **5**, 1825–1830.
93 C. Hu, C.-Y. Hung, K.-H. Chang and Y.-L. Yang, *J. Power Sources*, 2011, **196**, 847–850.
94 T. Weigert, Q. Tian and K. Lian, *J. Power Sources*, 2011, **196**, 4061–4066.
95 J. Eskusson, A. Jänes, A. Kikas, L. Matisen and E. Lust, *J. Power Sources*, 2011, **196**, 4109–4116.
96 J. Bae, M. K. Song, Y. J. Park, J. M. Kim, M. Liu and Z. L. Wang, *Angew. Chem., Int. Ed.*, 2011, **50**, 1683–1687.
97 C. D. Lokhande, D. P. Dubal and O.-S. Joo, *Curr. Appl. Phys.*, 2011, **11**, 255–270.
98 C. Chuang, C. Huang, H. Teng and J. Ting, *Compos. Sci. Technol.*, 2012, **72**, 1524–1529.
99 X. Zhang, Q. He, H. Gu, H. A. Colorado, S. Wei and Z. Guo, *ACS Appl. Mater. Interfaces*, 2012, **5**, 898–910.
100 H. Wei, X. Yan, S. Wu, Z. Luo, S. Wei and Z. Guo, *J. Phys. Chem. C*, 2012, **116**, 25052–25064.
101 S. Wei, P. Mavinakuli, Q. Wang, D. Chen, R. Asapu, Y. Mao, N. Haldolaarachchige, D. P. Young and Z. Guo, *J. Electrochem. Soc.*, 2011, **158**, K205–K212.
102 K. Ding, H. Jia, S. Wei and Z. Guo, *Ind. Eng. Chem. Res.*, 2011, **50**, 7077–7082.
103 D. Dubal, S. Patil, A. Jagadale and C. Lokhande, *J. Alloys Compd.*, 2011, **509**, 8183–8188.
104 H. Wei, H. Gu, J. Guo, S. Wei, J. Liu and Z. Guo, *J. Phys. Chem. C*, 2013, **117**, 13000–13010.
105 H. Wei, H. Gu, J. Guo, S. Wei and Z. Guo, *J. Electrochem. Soc.*, 2013, **160**, G3038–G3045.
106 H. Wei, J. Zhu, S. Wu, S. Wei and Z. Guo, *Polymer*, 2013, **54**, 1820–1831.
107 X. Zhou, C. Shang, L. Gu, S. Dong, X. Chen, P. Han, L. Li, J. Yao, Z. Liu and H. Xu, *ACS Appl. Mater. Interfaces*, 2011, **3**, 3058–3063.
108 Y. Wu, J. Yu, H.-M. Liu and B.-Q. Xu, *J. Nanosci. Nanotechnol.*, 2010, **10**, 6707–6719.
109 D. Priftis, N. Petzetakis, G. Sakellariou, M. Pitsikalis, D. Baskaran, J. W. Mays and N. Hadjichristidis, *Macromolecules*, 2009, **42**, 3340–3346.
110 A. R. Unnithan, N. A. M. Barakat, R. Nirmala, S. S. Al-Deyab and H. Y. Kim, *Ceram. Int.*, 2012, **38**, 5175–5180.
111 X. Peng, A. C. Santulli, E. Sutter and S. S. Wong, *Chem. Sci.*, 2012, **3**, 1262–1272.
112 Q. Shi, C. Jiang, Y. Wang, W. Yang and C. Yang, *Appl. Surf. Sci.*, 2013, **273**, 769–775.
113 A. Bokare, M. Pai and A. A. Athawale, *Sol. Energy*, 2013, **91**, 111–119.

114 L. Kong, G. Duan, G. Zuo, W. Cai and Z. Cheng, *Mater. Chem. Phys.*, 2010, **123**, 421–426.
115 B. Palanisamy, C. M. Babu, B. Sundaravel, S. Anandan and V. Murugesan, *J. Hazard. Mater.*, 2013, **252–253**, 233–242.
116 J. Niu, B. Yao, Y. Chen, C. Peng, X. Yu, J. Zhang and G. Bai, *Appl. Surf. Sci.*, 2013, **271**, 39–44.
117 R. Sasikala, A. Shirole, V. Sudarsan, T. Sakuntala, C. Sudakar, R. Naik and S. R. Bharadwaj, *Int. J. Hydrogen Energy*, 2009, **34**, 3621–3630.
118 M. F. Abdel-Messih, M. A. Ahmed and A. S. El-Sayed, *J. Photochem. Photobiol., A*, 2013, **260**, 1–8.
119 R. S. Barhate and S. Ramakrishna, *J. Membr. Sci.*, 2007, **296**, 1–8.
120 S. Chigome and N. Torto, *Anal. Chim. Acta*, 2011, **706**, 25–36.
121 J. Lev, M. Holba, L. Kalhotka, M. Szostkova and D. Kimmer, Proc. Int. Conf., NANOCON, 2011.
122 S. S. Lee, H. Bai, Z. Liu and D. D. Sun, *Water Res.*, 2013, **47**, 4059–4073.

